



ELSEVIER

Available online at [www.sciencedirect.com](http://www.sciencedirect.com)

SCIENCE @ DIRECT®

Nuclear Instruments and Methods in Physics Research A 550 (2005) 616–625

NUCLEAR  
INSTRUMENTS  
& METHODS  
IN PHYSICS  
RESEARCH  
Section A

[www.elsevier.com/locate/nima](http://www.elsevier.com/locate/nima)

# POLAR, a compact detector for gamma-ray bursts photon polarization measurements

N. Produit<sup>a,\*</sup>, F. Barao<sup>b</sup>, S. Deluit<sup>a</sup>, W. Hajdas<sup>c</sup>, C. Leluc<sup>d</sup>, M. Pohl<sup>d</sup>, D. Rapin<sup>d</sup>, J.-P. Vialle<sup>e</sup>, R. Walter<sup>a</sup>, C. Wigger<sup>c</sup>

<sup>a</sup>ISDC, Université de Genève, Switzerland

<sup>b</sup>LIP, Lisboa, Portugal

<sup>c</sup>PSI, Villigen, Switzerland

<sup>d</sup>DPNC, Université de Genève, Switzerland

<sup>e</sup>LAPP/IN2P3/CNRS, Annecy, France

Received 28 February 2005; received in revised form 3 May 2005; accepted 4 May 2005

Available online 7 July 2005

## Abstract

The design and the simulated performances of a compact detector dedicated to the measurement of GRB photon polarization is presented. Such a detector would permit to answer the question “are most of the GRB strongly polarized?” in a mission of one year in space.

© 2005 Elsevier B.V. All rights reserved.

PACS: 98.70.RZ; 29.40.Mc; 95.55.Ka

Keywords: Gamma-ray; Gamma-ray astronomy; Polarimetry; Polarization; Gamma-ray burst; Crab

## 1. Introduction

Discovered 35 years ago, Gamma-Ray Bursts (GRB) remain a challenging issue and one of the most interesting topics in astrophysics. The genuine character of the GRB sources and the energy release mechanisms still remain a mystery

and there are several competing theoretical models and mechanisms trying to explain it.

The launch of several high energy observatories with powerful instruments on board (XMM, Integral, RHESSI, BeppoSax) and of advanced GRB detectors (CGRO, HETE2) made possible a number of new discoveries and in parallel noteworthy theoretical progresses. However the instruments advances were mainly on effective area, energy and angular resolution, while very little progress was achieved on polarization measure-

\*Corresponding author. Tel.: +41 22 379 2140; fax: +41 22 379 2133.

E-mail address: [nicolas.produit@obs.unige.ch](mailto:nicolas.produit@obs.unige.ch) (N. Produit).

ment, partly due to the experimental difficulty of measuring polarization. Today, photon polarization turns out to be one of the ultimate observables required to make a clear distinction between different theoretical models in order to fully understand the GRB nature. To date however, the polarization was explored only in a few afterglow measurements in visible light.

The recent report [1] of a high linear polarization ( $80 \pm 20\%$ ) in the prompt emission of GRB021206, together with its subsequent revisions as too preliminary (if not mistaken) [2,3], demonstrated that polarimetric measurements are difficult and need dedicated instruments. Such measurements are a must in the era of missions like SWIFT [4] or the forthcoming GLAST [5] experiment. Both SWIFT and GLAST can promptly determine the exact GRB coordinates as well as the lightcurve and spectral characteristics. For such bursts the polarimetric detectors will bring simultaneously additional unique information about the magnetic field structure and dynamics during the prompt gamma-ray emission. We propose here a dedicated instrument with high sensitivity for polarization measurements.

## 2. GRBs and polarization

Many theoretical models of GRBs give polarization predictions for both, prompt and afterglow emissions [6–12]. The commonly accepted fireball model requires a fine tuning of the magnetic field structures in order to provide high values of polarization. In addition, it predicts similar polarization values for prompt and afterglow emissions. Other models, like the electromagnetic and the cannonball, allow for high polarization of photons in a more straightforward manner. As a matter of fact, predictions are not unique but rather give a range of polarization levels as, like in the cannonball model, the value of the polarization depends not only on internal parameters but also on the observer's viewing angle. Unambiguous distinction between models thus demands multiple polarization measurements from a large number

of bursts, which in turn implies a dedicated polarization detector.

It is extremely difficult to cover a wide energy range while getting the high detection sensitivity needed for the GRB studies within a single spacecraft instrumentation. Even the recently launched top-of-the-art GRB observatory SWIFT has a photon detection upper energy limit of about 150 keV, and it does not carry a gamma-ray polarimeter on board. At present, the GRB measurement approach is to conduct a number of multi-wavelength observations done both simultaneously and in a follow-up manner with multiple detector systems usually installed on different satellites linked together. Such a global network (GCN [13]) synchronizes various observations and provides in quasi real time GRB detection alerts to many follow-up instruments like optical telescopes. Though, despite of many attempts supported by wide theoretical efforts, polarization data remain very scarce and measurements very difficult. There are only few results reporting polarization measurements in the GRB afterglow data [14]. At typical gamma-ray energies, even novel instruments with designed polarimetric capabilities like e.g. RHESSI [15] with its passive Beryllium scatterer face problems with systematic effects. In coincidence mode, the RHESSI polarimeter has very small active area and suffers from either poor statistics or high background levels or both [3]. Other satellites like Integral [16] have their instruments not optimized for polarization measurements. Therefore, their efficiency, analyzing power or background suppression capability is too low for any meaningful long-term observations.

Bearing in mind the outstanding importance of polarization measurements, we propose a GRB polarimeter based on Compton scattering and on well known detection technologies. The design is optimized for an energy range from a few keV up to several hundred keV and a wide viewing angle. The instrument is characterized by a large area and high analyzing power. It utilizes low  $Z$ , fast scintillation square detector bars arranged in a large array. Full description of the polarimeter and first results from its extensive modeling are presented below.

### 3. Detector requirements

The method for measuring gamma-ray polarization depends on their energy. In the energy range of 10 keV to 1 MeV, Compton scattering can be used thanks to its large cross section and its sensitivity to polarization (see geometry in Fig. 1). Small angle scatterings dominate the total cross section, but they basically conserve the direction of polarization of the incoming photon, thus they do not affect the measurement. In large angle scatterings, the azimuthal ( $\xi$ ) angular distribution is strongly modulated around the photon polarization direction. It can be reconstructed by observing the recoil electron from the Compton scattering and then observing the scattered photon by a subsequent process depositing sufficient energy (second Compton scattering or photoelectric effect). In addition, the cross section is symmetric under  $\xi \rightarrow \pi - \xi$ , such that it is not necessary to know the order in time of the two observations. Monte Carlo simulation clearly indicate that it suffices to isolate the two most energetic processes. The line connecting them is well correlated with the outgoing azimuthal direction  $\xi$ .

In the design of the detector, the following key features must be taken into account:

- At X-ray and soft gamma-ray energies the radiation and the absorption lengths are short enough such that a rather compact detector using low  $Z$  materials is conceivable.
- The detector must tolerate multiple small angle scatters, favor large angle Compton scatterings, and offer a good resolution for the  $\xi$  angle.
- Charged particles, entering with an overwhelmingly high rate, must not leave a signal that could be confused with the desired photon signal.
- Photons from the spacecraft itself, from diffuse radiation and from usual sources form together an irreducible background. Signal-to-background ratio thus call for a fast detector response with good time resolution.

These considerations lead us to a design (See Fig. 2) consisting of an homogeneous and sym-

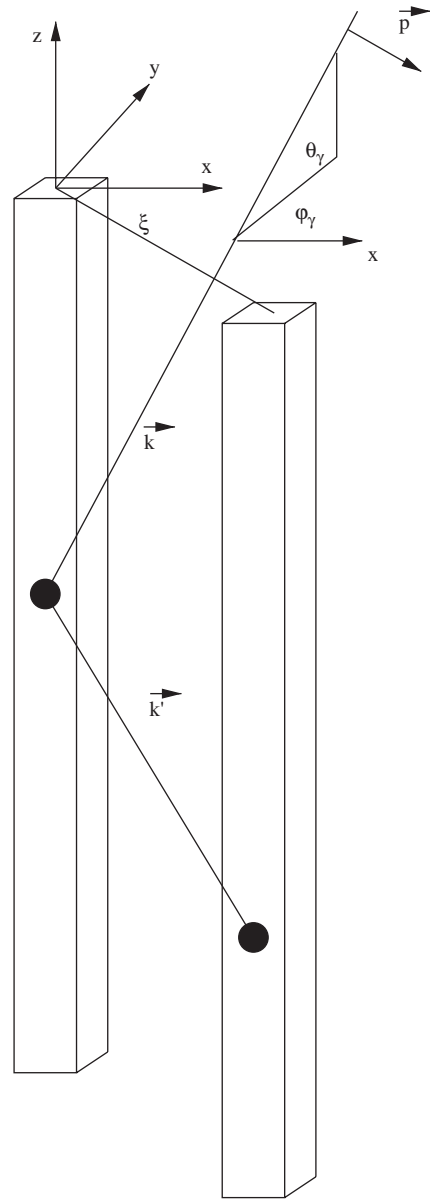


Fig. 1. Geometry of the large angle Compton scattering. The two bars where interaction occur are shown.  $\theta_\gamma$  and  $\phi_\gamma$  are the entrance angle of the photon relative to a detector fixed coordinate system.  $\xi$  is the measured azimuthal direction that correlate with polarization direction  $\vec{p}$ .

metric active target, made of not very high  $Z$  material, like plastic scintillator. A target segmentation of a few  $\text{mm}^2$  was dictated by the range of

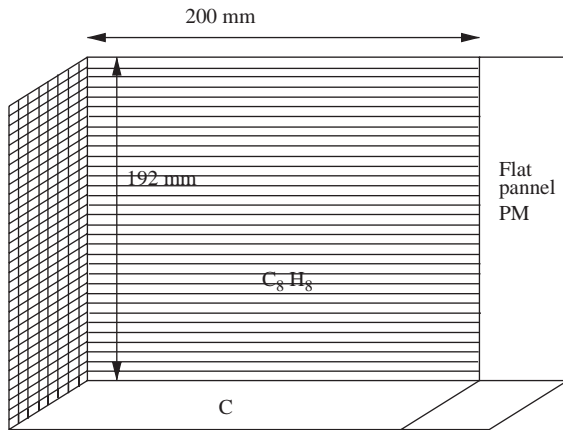


Fig. 2. Schematic view of the POLAR detector.

recoil electrons in the given photon energy range as well as the required angular resolution. This segmentation matches well the anode dimensions of modern metal mesh multi-anode photo multipliers (PM), which have already found widespread use in space missions and provide the performances required.

#### 4. The POLAR detector

The detector is an active target of outer dimensions  $192 \times 192 \times 200 \text{ mm}^3$ . The target material is plastic scintillator, i.e. doped polystyrene, chemically and mechanically stable and supporting high total radiation doses with little degradation. The target is segmented into 2304 elements of dimension  $4 \times 4 \times 200 \text{ mm}^3$ , with their long axis facing the preferred photon entry direction. The target elements are optically insulated from each other by applying a thin double layer of reflective/diffusive paint.

The front face of the target is shielded by a 1 mm carbon fiber shield to absorb very low energy photons and charged particles. Likewise the sides are passively shielded by a 1 mm thick carbon fiber, which also provides a mechanical enclosure. On the back, a flat panel metal mesh photo detector is directly coupled to the scintillator elements. With the associated power distribution and front-end electronics, the photo detector is

thick enough to shield the detector from photons entering from the back.

#### 5. Trigger strategy

The signal for a Compton scattering consists of at least two energy depositions, from the recoil electron in a large angle scatter and from a subsequent photon interaction via additional Compton scattering or photoelectric effect. The trigger logic thus requires at least two coincident channels each with at least 5 keV energy deposition. The two elements with the highest energy deposits define the geometry of the event. The photon entrance angles are assumed to be known, they are derived from the knowledge of the spacecraft attitude and from the GRB sky coordinates given by another spacecraft or the GCN. The azimuthal angle of the straight line connecting the two highest energy hits around the entrance axis thus defines the  $\zeta$  angle sensitive to polarization. There is no requirement of maximum distance between the two highest energy deposits, but a criterion could be defined without large acceptance losses (see Fig. 3).

A charged cosmic ray traversing the detector will hit several plastic bars and deposit in each of them at least 800 keV. To get rid of this background the trigger requires that the total energy deposition in the target is less than 300 keV. This cut has little effect on the signal photons

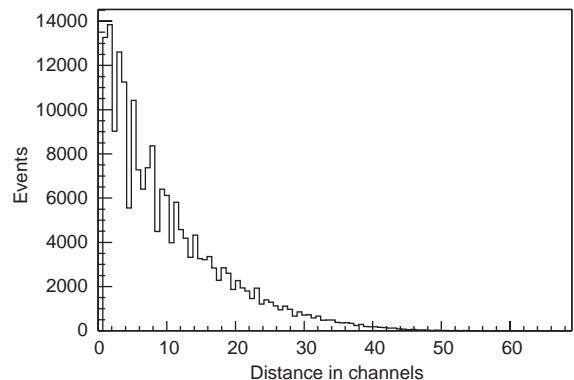


Fig. 3. Distance in scintillator elements width between the two largest energy deposition.

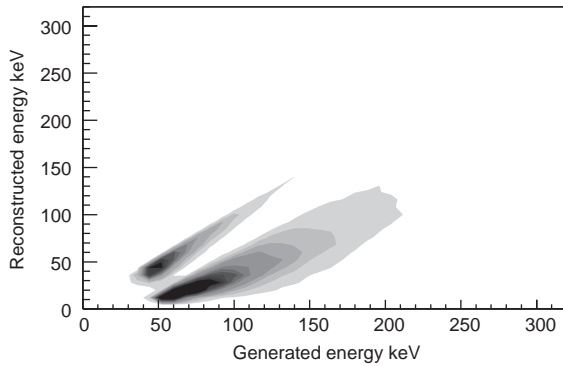


Fig. 4. Primary energy (abscissa) vs reconstructed deposited energy (ordinate). Diagonal events are fully contained. For most of the events (the lower population), some energy escapes the detector.

(see Fig. 4), since the photon energy spectrum of GRBs is steep, and the detectability of polarization favors low energy photons.

Using a typical light yield of 1 photon/90 eV, 5 keV primary energy deposition corresponds to about 55 primary scintillation photons. A conservative light collection efficiency of 10% and a typical quantum efficiency of 0.2 shows that an electronics sensitive to single photoelectrons will reach this threshold. A lower threshold is not desirable as the background increase faster than the signal for low energies.

## 6. Physics simulation

The interactions of signal and background photons with the detector has been simulated using GEANT 4 [17]. The target is simulated as a solid block of  $C_8H_8$  material with appropriate density and radiation length. The high voltage divider and electronics material on the back end of the target was grossly approximated as a 10 cm deep block of aluminum with reduced density ( $0.9 \text{ g cm}^{-3}$ , i.e. 1/3 of pure aluminum). The front and side shield are taken as 1 mm of carbon of density  $2.265 \text{ g cm}^{-3}$ . The total weight of the detector simulated is then 11.4 kg.

Incoming photons have been generated uniformly over the front surface, with entrance angles

of  $0^\circ \leq \theta_\gamma < 70^\circ$  and  $\phi_\gamma = 0^\circ$  or  $45^\circ$ . Photons generated are fully polarized with a polarization vector  $\phi_0 = 0$  parallel to one of the detector faces, but it has been checked that the results of the study remain valid for other directions. The energy is sampled from a distribution based on a band model [18] with parameters  $\alpha = -1$ ,  $\beta = -2.5$  and  $E_{\text{peak}} = 200$ , between 10 and 300 keV. The corresponding spectrum is shown in Fig. 5, compared to a typical background distribution (see Section 7).

The simulation of physics processes includes the polarization dependence of Compton scattering, and takes into account the electromagnetic processes which are all implemented in GEANT 4, even those at very low energy. As expected, the photon interactions are dominated in number by low energy Compton scattering with small energy transfer to the electron. Whenever a large angle scattering occurs, a clear modulation of the azimuthal angle is observed. On average, 14% of the events fulfill the double energy deposition coincidence required by the trigger.

Fig. 3 shows the distance between the two largest energy depositions in units of element width. The leveling off of the distribution justifies the target dimensions. Since there are few entries at large distances, a maximum distance requirement can be introduced if required by combinatorics, at the cost of a small efficiency loss.

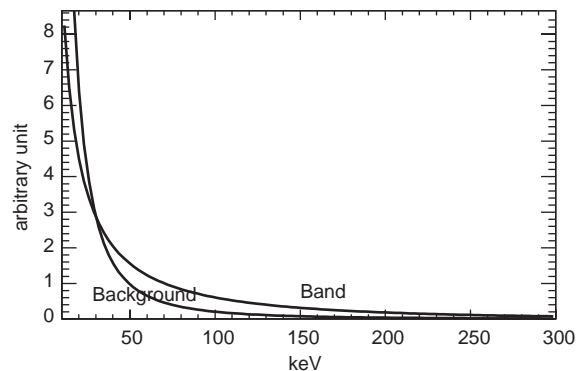


Fig. 5. Band function used to simulate the photon spectrum emitted by GRBs. For comparison the distribution of diffuse background is plotted scaled to the same integral flux in the energy range between 10 and 300 keV.

Fig. 4 shows the reconstructed total energy in the target versus the energy of the incoming photon. It is clearly seen that for a fraction of the events the full energy is collected while for others only a large angle Compton scattering deposition occurs, the outgoing photon escaping from the detector.

As an example, Fig. 6 shows the reconstructed azimuthal angle distribution for a very intense GRB. For a polarization orientation along  $\xi_0 = 0^\circ$ , the maximum signal rate should be at  $90^\circ$ , which is indeed observed. The observed rate as a function of  $\xi$  during a fixed time interval of the burst is parameterized as  $dN/d\xi = A(1 + B \cos 2(\xi - \xi_0))$ . The modulation B indicates the degree of polarization, while the phase  $\xi_0 - \pi/2$  indicates the polarization orientation.

The effective area, given by the geometrical surface multiplied by the photon detection probability, varies from 100 to  $40 \text{ cm}^2$ , depending on the photon entrance angle. As shown in Fig. 7, the acceptance varies slowly over about  $1.3\pi \text{ sr}$ . Within this fiducial solid angle the average area is  $80 \text{ cm}^2$ .

Depending on photon energy and impinging angle, the modulation varies from 0.34 to 0.2, as shown in Fig. 8. In further estimates, an average modulation of 0.28 will be used.

Fig. 9 shows the measured polarization orientation and the error on the degree of polarization in function of the intensity of the GRB. If the flux is not sufficient, no measurement of polarization is

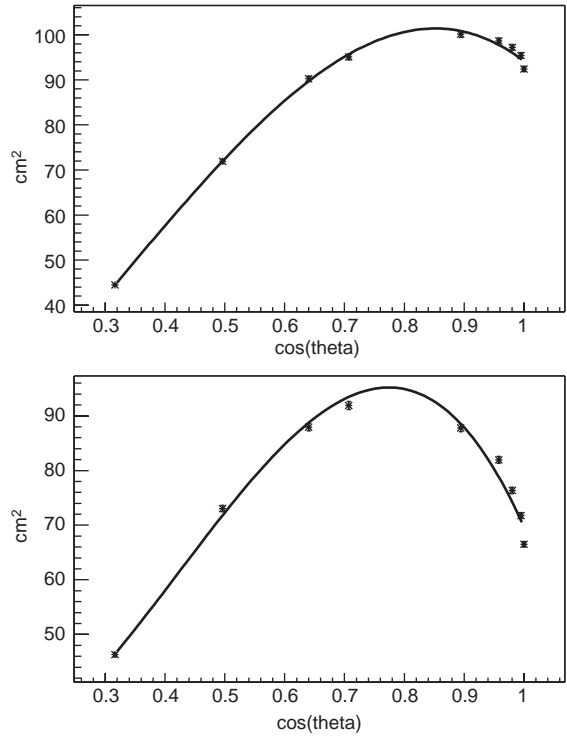


Fig. 7. Effective surface of the detector in  $\text{cm}^2$  for photons with energies between 10 and 300 keV as a function of  $\cos \theta_\gamma$  for  $\phi_\gamma = 0$  and  $45^\circ$ .

possible but there is no systematic bias in the measurement as seen on Fig. 10.

### 7. Background estimate

Table 1 summarizes the expected trigger rate from the different processes of signal and background and their impact on the dead time of the detector. When a signal  $> 5 \text{ keV}$  induce a signal in one or many PM channels, those channels go dead for 100 ns (PM hits). When a coincidence of at least two PM with proper energy range hits occur, the detector is read out.

High energy charged particle background is eliminated completely by the upper energy cut in the trigger. They induce PM hits but no readout and no dead time. Induced beta and alpha radioactivity is also not likely to pass the trigger selection except if they take place exactly between

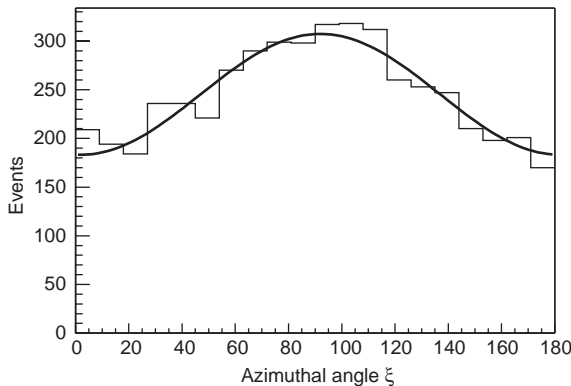


Fig. 6. Example of a modulation curve measurement for a very intense signal.

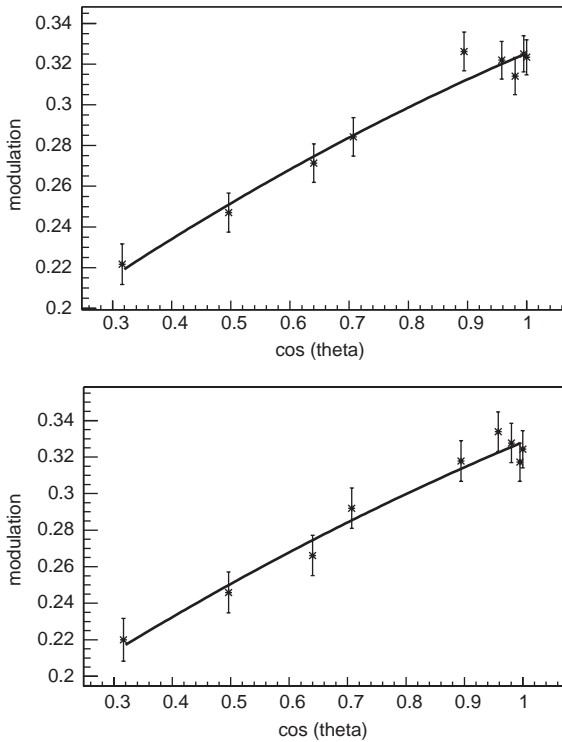


Fig. 8. Modulation of the azimuthal angle distribution as a function of the photon polar angle  $\cos(\theta_\gamma)$  for  $\phi_\gamma = 0$  and  $45^\circ$ . For typical entrance angles, a mean modulation of about 0.28 is expected.

two bars. If they turn out to be a problem we can eliminate them with a cut excluding adjacent bars with a low penalty as can be seen on Fig. 3. Low energy electrons from the radiation belts are a more serious nuisance. Electron under 500 keV are stopped by the 1 mm carbon shield. Electrons between 50 keV and 1.5 MeV have a  $10^{-3}$  probability to look like a real event (d in the table). They are so numerous that a random coincidence of two of them is likely (noted  $r$  in the table). An orbit like the ISS is spending 20% of the time in the polar horns and in the South Atlantic anomaly. When in those region the detector will receive  $10^3 \text{ cm}^{-2} \text{ s}^{-1}$  electrons in this range. If they turn out to be a real nuisance, the detector will be switched off when crossing those regions. All other electrons are vetoed by the trigger.

Protons from the belt are no problems. Protons  $< 13 \text{ MeV}$  do not enter the sensitive volume.

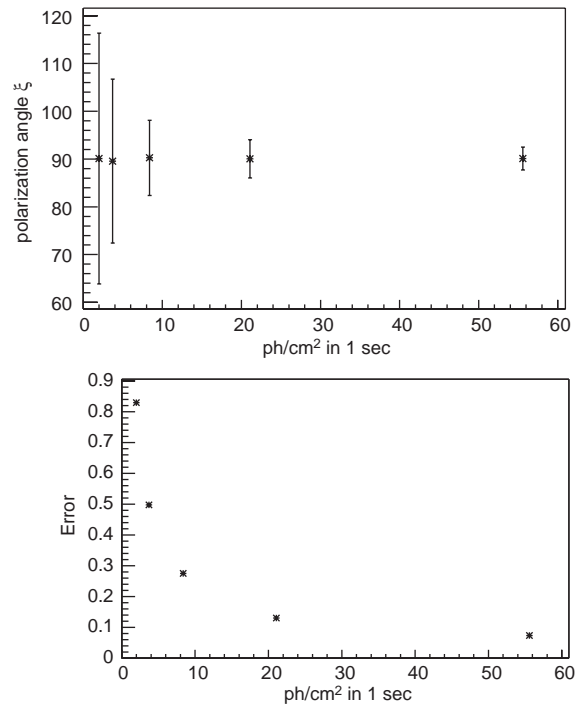


Fig. 9. Polarization orientation  $\xi_0$  and reconstructed error on the degree of polarization as a function of the GRB flux during a 1 s interval.

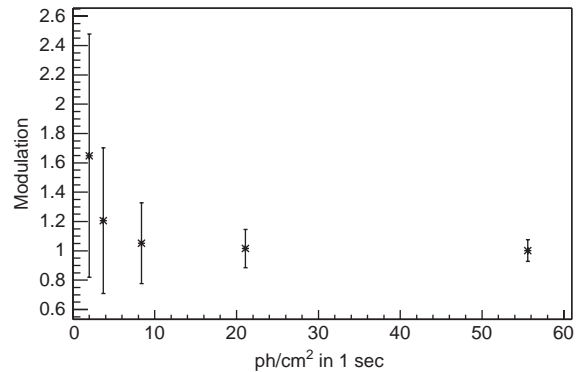


Fig. 10. Mean value and r.m.s. of the reconstructed degree of polarization, extracted from a large sample of simulated GRB. At measurable degrees of polarization, the measurement is unbiased and exhaustive.

Proton  $> 13 \text{ MeV}$  are rejected by the trigger. In the polar horns and South Atlantic anomaly there is about  $10 \text{ protons cm}^{-2} \text{ s}^{-1}$  of energy greater than 13 MeV.

Table 1

The different processes contributing to signal and background and their impact on the trigger rate

| Process            | Flux   | Rate Hz           | PM hits Hz        | Readout rate Hz   |
|--------------------|--|-------------------|-------------------|-------------------|
| Strong GRB         | $20 \text{ cm}^{-2} \text{ s}^{-1}$                      | $8 \times 10^3$   | $4 \times 10^3$   | $1.6 \times 10^3$ |
| Diffuse $\gamma$   | $2.46 \text{ cm}^{-2} \text{ s}^{-1} \text{ sr}^{-1}$    | $1.8 \times 10^4$ | $5 \times 10^3$   | 430               |
| Cosmic             | $10^{-1} \text{ cm}^{-2} \text{ s}^{-1} \text{ sr}^{-1}$ | 700               | 700               | 0                 |
| Proton < 13 MeV    | $10^3 \text{ cm}^{-2} \text{ s}^{-1}$                    | $2.8 \times 10^6$ | 0                 | 0                 |
| Proton > 13 MeV    | $10^2 \text{ cm}^{-2} \text{ s}^{-1}$                    | $2.8 \times 10^5$ | $2.8 \times 10^5$ | 0                 |
| Electron < 500 keV | $10^5 \text{ cm}^{-2} \text{ s}^{-1}$                    | $2.8 \times 10^8$ | 0                 | 0                 |
| Electron > 500 keV | $310^3 \text{ cm}^{-2} \text{ s}^{-1}$                   | $9 \times 10^6$   | $5 \times 10^6$   | 400 d + 50 r      |

Flux is the theoretical flux. Rate is the flux integrated over the fiducial surface. PM hits is the number of time a PM signal pass the lower threshold, this incurred a 10 ns dead time. The readout rate is number of time a coincidence in the correct energy window occur.

There are four sources of background of photons: (i) induced radioactivity in the scintillator (ii) induced radioactivity in the supporting spacecraft (iii) non-GRB point sources and (iv) the diffuse  $\gamma$  ray flux. Induced  $\gamma$  rays flux depend very much on the orbit and on the design of the spacecraft. As a rough estimate we shall take these numbers from the Integral mission. In the ISGRI instrument of Integral, there is a background of  $0.02 \text{ photons cm}^{-2} \text{ s}^{-1} \text{ sr}^{-1}$  in a similar energy range.

The diffuse photon background from the sky has been parameterized [19] as  $\log f(E) = a + b \log E + c \log E \log E$  photons  $\text{cm}^{-2} \text{ s}^{-1} \text{ sr}^{-1} \text{ keV}^{-1}$ , with  $a = 0.940059$ ,  $b = -1.28089$ ,  $c = -0.262414$  and  $E$  in keV. This parameterization predicts  $2.46 \text{ photons cm}^{-2} \text{ sr}^{-1} \text{ s}^{-1}$  with  $E_\gamma > 10 \text{ keV}$ . A source like the Crab, with a flux of  $9.7(E/1\text{keV})^{-2.1}$  photons  $\text{cm}^{-2} \text{ s}^{-1} \text{ keV}^{-1}$  is contributing  $0.7 \text{ photons cm}^{-2} \text{ s}^{-1}$  in the energy range from 10 to 300 keV.

### 7.1. Sensitivity to background photons

Photons distributed like the diffuse background between 10 and 300 keV, coming from the  $2\pi \text{sr}$  of sky above the detector have been simulated. The acceptance for these photons has been found to be  $175.2 \text{ cm}^2 \text{ sr}$ . The reconstructed polarization angle has a structure incompatible with the signal. As the detector is a cube we expect to see a modulation with period  $\pi/2$ . Therefore the background has been fitted with a function  $dN/d\xi =$

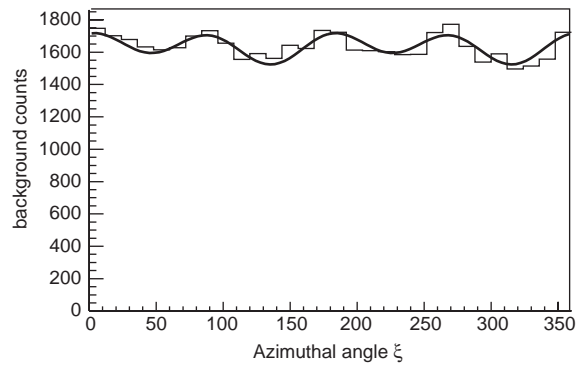


Fig. 11. Azimuthal angle distribution of background photons. The detector geometry induces a modulation with a  $\pi/2$  periodicity with respect to one of its axes, which is easy to model and subtract.

$A(1 + B \cos 4(\xi - \xi_0) + C \cos 2(\xi - \xi_1))$  as it is shown in Fig. 11.

Using the efficiency found for photons distributed according to such an energy distribution, a background rate of  $430 \text{ counts s}^{-1}$  is predicted in the target.

## 8. Minimum detectable polarization levels

A toy Monte Carlo calculation was used to estimate the minimum polarization detectable. Neglecting the modulation induced by the target geometry, a flat background superimposed with events distributed like a 100% polarized GRB has been made. Statistical fluctuations of the back-

ground and of the signal rate has been properly taken into account. A maximum likelihood fit to the distribution has been used for extracting the modulation as well as the phase angle.

The minimum detectable polarization level can be defined as  $MDP = n_\sigma / \mu S \sqrt{(S+B)/T}$  with  $n_\sigma$  is the number of  $\sigma$  we want for our signal,  $S$  the signal rate,  $B$  the background rate and  $\mu$  the modulation for a 100% polarized signal. With this formula using  $n_\sigma = 3$ ,  $\mu = 0.28$ ,  $B = 430 \text{ photons}^{-1}$  and an effective area of  $80 \text{ cm}^2$ , a MDP of 100% is reached with a peak flux of  $3.6 \text{ photons cm}^{-2} \text{ s}^{-1}$  in a 1 s measurement.

### 8.1. Sensitivity to GRB

According to the GUSBAD catalog [20] there are 250 burst per year with a peak flux  $> 1 \text{ photon cm}^{-2} \text{ s}^{-1}$  in the BATSE energy range 50–300 keV. Extrapolation to our energy range (10–300 keV) gives a factor 2.5 bigger flux. Fig. 12 show the minimum detectable polarization level in a GRB in function of the mean waiting time in days for the occurrence of such a GRB according to the GUSBAD catalog and taking into account that only  $\frac{1}{3}$  events are in our acceptance.

The duration of GRB is very variable. For short bursts which last less than 2 s, the signal to background ratio is good enough even for low fluences. For intense long duration bursts, a polarization measurement in time slices

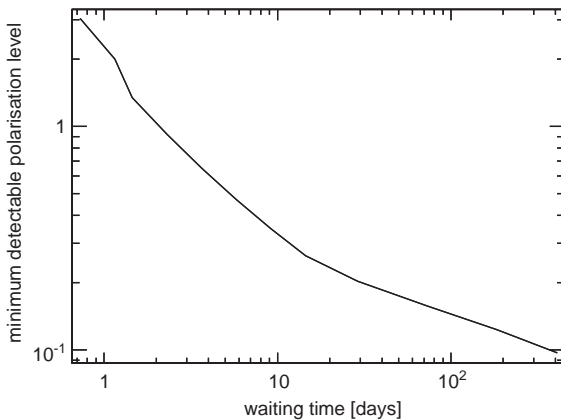


Fig. 12. Minimum detectable polarization level in function of waiting time.

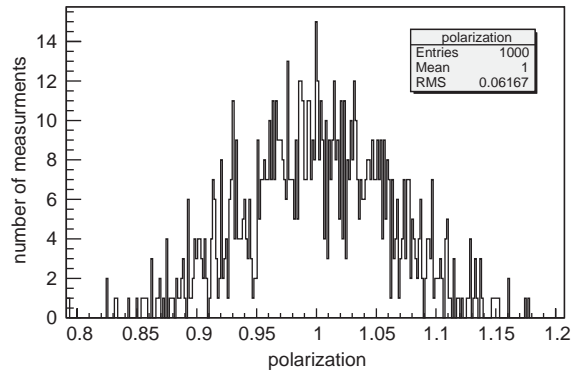


Fig. 13. Reconstructed degree of polarization for photons from the Crab nebula, assuming 1000 measurements of 1000 s duration, assuming 100% polarized photons from the source.

of a few seconds is promising. Such a measurement is important since polarization could vary time.

### 8.2. Sensitivity to the Crab nebula

While the crab nebula is in the field of view of POLAR, a continuous polarization measurement is feasible. In a 1 ks exposure, POLAR will collect about 56000 photons from the crab over a mean of  $430000 \pm 655$  photons of background. The expected results from 1000 such measurements are represented in Fig. 13. With the formula for the minimum detectable polarization level we see that to detect a 1% polarization of the Crab we need to measure it for 180 ks.

## 9. Conclusions

Polarization is one the missing key to test different theoretical models of GRB. We have presented the design of a compact (12 kg) detector to measure the polarization of GRB. With that instrument we will know after one month of mission if highly polarized GRB exists. In case GRB are not polarized, a limit down to 10% polarization will be obtained after one year. An array of such detector can be envisaged for increasing the polarization sensitivity or the angular coverage.

**References**

- [1] W. Coburn, S.E. Boggs, *Nature* 423 (2003) 415–417.
- [2] R.E. Rutledge, D.B. Fox, *Mon. Not. Roy. Astron. Soc.* 350 (2004) 1272.
- [3] C. Wigger, et al., *Astrophys. J.* 613 (2004) 1088–1100.
- [4] N. Gehrels, *AAS*, vol. 195, No. #92.08.
- [5] A. de Angelis, in: A.M. Mourao, M. Pimenta, P.M. Sa, J.M. Velinho (Eds.), *Proceedings of the Third International Workshop on New Worlds in Astroparticle Physics*, ISBN: 9810247079, p. 140.
- [6] S. Dado, A. Dar, A. De Rujula, astro-ph/0403015
- [7] B. Zhang, et al., *Astrophys. J.* 595 (2003) 950–954.
- [8] M. Lyutikov, et al., *Astrophys. J.* 597 (2003) 998–1009.
- [9] D. Eichler, A. Levinson, *Astrophys. J.* 596 (2003) L147–L150.
- [10] E. Nakar, et al., *JCAP* 10 (2003) 005.
- [11] J. Granot, *The Astrophys. J.* 596 (2003) L17–L21.
- [12] D. Besset, et al., *Nucl. Instr. and Meth. A* 166 (1979) 515–520.
- [13] S. Barthelmy, *Gamma-ray bursts. 4th Huntsville Symposium, AIP Conference Proceedings* 428, 1998, pp. 99–103.
- [14] S. Covino, et al., *Astron. Astrophys.* 400 (2003) L9.
- [15] R.P. Lin, et al., *Sol. Phys. A* 210 (2002) 3.
- [16] P. Ubertini, *Astron. Astrophys.* 411 (2003) L131–L139.
- [17] S. Agostinelli, et al., *Nucl. Instr. and Meth. A* 506 (2003) 250–303.
- [18] D. Band, et al., *Astrophys. J.* 413 (1993) 281–292.
- [19] Oliver Grimm, Ph.D. Thesis, Dissertation ETH No. 14576, Zuerich, March 2002.
- [20] M. Schmidt, *Astrophys. J.* 616 (2004) 1072–1077.